Structuration of the Solar Plasma by the Magnetic Field

Pascal Démoulin and Karl-Ludwig Klein

Observatoire de Paris, Section de Meudon, DASOP, URA 2080 (CNRS), F-92195 Meudon Cedex, France; e-mail: demoulin@obspm.fr, klein@obspm.fr

Abstract. This paper presents a simplified overview of the role of the magnetic field in the solar atmosphere. The magnetic field emanating from the solar interior governs energy transport and plasma motions in the outer solar atmosphere. Thereby it creates structure, such as coronal holes, loops and prominences, and the dynamical phenomena known as coronal mass ejections and flares. The magnetic field is also thought to be at the origin of the coronal heating, so of the corona itself. An overview of atmospheric structure is presented, followed by illustrations on present ideas on the interaction between plasma and magnetic field. The physical conditions in the corona are briefly compared to those in the magnetosphere. The emphasis is then put on the energetic processes from the largest ones (coronal mass ejections) over flares and X-ray bright points to coronal heating. In all cases magnetic reconnection is likely to play a key role. Solar prominences are then described because their observations provide important information on the surrounding coronal magnetic field. Finally the implications of processes in the convection zone on the physics of the corona and of the interplanetary medium are illustrated for the case of formation, storage and ejection of twisted magnetic flux tubes.

1 Introduction

Solar magnetic fields are created at the bottom of the convection zone from the kinetic energy of the dense plasma. Buoyant flux tubes rise into the atmosphere, such that the magnetic field eventually fills the corona, creates its structures and governs its dynamics. This provides energy transport into the atmosphere, where the interaction between the plasma and the magnetic field leads to dynamical phenomena including heating, particle acceleration and the ejection of material.

The term "atmosphere" designates the outer envelope of the Sun, where the electromagnetic radiation is generated. Section 2 of this review presents the basic temperature regimes of the atmosphere (photosphere, chromosphere, corona), outlines the different types of electromagnetic radiation, and illustrates the most important plasma structures in the (low-beta) corona that we interpret as being generated by the magnetic field.

Present ideas on the interaction of plasma and magnetic fields in the corona are discussed for selected topics in the following Sections. Emphasis is laid on the structure and evolution of the magnetic field configurations.

The physical system is always described by MHD equations (see e.g. Heyvaerts 1998). Each selected topic is treated in two basic parts: the first is general, introducing the subject, and the second focuses on one aspect of present research. Several textbooks treat these subjects with more detail: Stix (1991) provides an introduction to solar physics with emphasis on the interior and low atmosphere. Tutorial lectures and reviews on all fields of solar physics are presented in the books edited by Cox et al. (1991) and Schmelz and Brown (1992). Priest (1982) is a classical monograph providing both a summary of observations and models with emphasis on the solar atmosphere viewed from the MHD point of view. The solar corona has been recently reviewed by Golub and Pasachoff (1997). A review based mostly on white-light and radio sounding observations of large-scale properties is Bird and Edenhofer (1990). Flares and filaments have been described in detail by Tandberg-Hanssen and Emslie (1988) and Tandberg-Hanssen (1995), respectively. Coronal mass ejections are reviewed in the book edited by Crooker, Joselyn and Feynman (1997). For kinetic aspects of solar and stellar coronae, which are not discussed here, the reader is referred to Benz (1993).

The release of magnetic energy in the corona occurs over a broad range going from 10^{25} J within minutes to hours (large flares, coronal mass ejections), possibly down to tiny and yet undetectable events such as Parker's suspected nanoflares (10^{16} J). One main, but not the only, process invoked is magnetic reconnection, which has been extensively studied in 2-D (see e.g. Parnell 1998). This approach has highlighted the importance of magnetic topology (Section 4.1). Recent works have evolved from 2D to 3D reconnection, giving a completely new view; this is shortly summarized to describe the energy release from the most spectacular events of large-scale magnetic restructuring (coronal mass ejections, in Section 4.2) to small-scale phenomena including flares (Section 4.3), X-ray bright points (Section 4.4), and coronal heating (Section 4.5). The prominences / filaments are then described in Section 5 because of their particular plasma structuration and because they provide important information on the surrounding coronal magnetic field. Finally in Section 6, an attempt is presented to link a part of the physics of the convective zone, of the corona and of the interplanetary medium.

2 The Structure of the Solar Atmosphere

2.1 General Aspects and Temperature Regimes

The schematic evolution of temperature with height in the solar atmosphere is plotted in Fig. 1. The *photosphere* is the deepest layer directly observable through its electromagnetic radiation (mainly visible light). The level of zero altitude ("bottom" of the photosphere) is defined as the height where the optical depth of radiation at 500 nm wavelength is unity. The temperature of the black body which gives the closest approach of the observed intensity spectrum of the radiation is $\sim$5700 K, but local temperature depressions

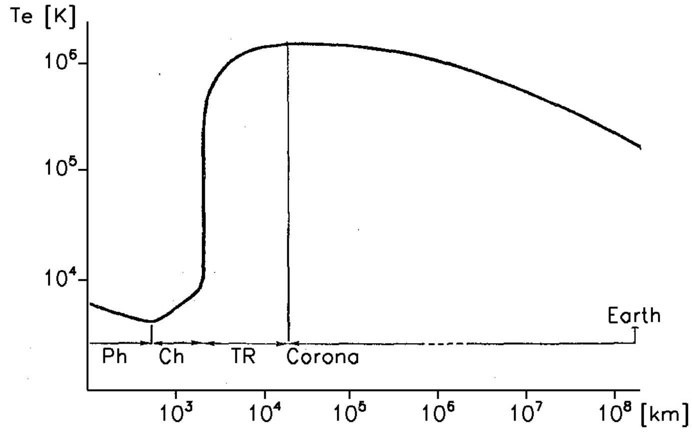

Fig. 1. Evolution of the electron temperature in the solar atmosphere as a function of height above the photosphere. The curve gives a schematic view of an "average" quiet atmosphere. Ph=photosphere, Ch=chromosphere, TR=transition region

(e.g. sunspots) and enhancements (faculae) by up to 1000 – 2000 K exist. Temperature first decreases with increasing altitude to a minimum of about 4400 K ("top" of the photosphere), over a distance of some hundreds of km. The cooler gas in the upper photosphere creates many absorption lines in visible light which are superposed upon the blackbody spectrum. Doppler and Zeeman effect measurements of these lines give the basic information on material flows and magnetic fields which govern the structure and dynamics of the overlaying atmosphere.

Above the photosphere temperature rises with increasing altitude. The region between the temperature minimum and $\sim$ 25 000 K is called the *chromosphere* because its optical and UV emission lines create a colored ring around the lunar disk during an eclipse. Besides in UV, the chromosphere can be observed in optical absorption lines (e.g. Hα) and at short radio wavelengths: the electron density in the atmosphere far from active regions is such that radio emission generated by free-free transitions (acceleration of free electrons by the electrostatic field of ions) can escape at frequencies above a few GHz (centimeter wavelengths). The thickness of the chromosphere is between one and a few thousand km.

The *corona* is the outer region of the atmosphere, with temperatures $\geq 10^6$ K. The narrow region between the upper chromosphere and the corona is called the (chromosphere-corona) *transition region*. The corona is visible in white light due to the scattering of photospheric light by free electrons ("K-corona") and dust ("F-corona"). Coronal emission comprises spectral lines of highly ionized heavy elements in visible, UV and EUV (especially Fe and Ca), as well as continuum emission (X, radio) due to free electrons. In the presence of strong magnetic fields, i.e. in the low corona above sunspots, centimetric cyclotron radio emission at low (2 to 4) harmonics of the electron cyclotron frequency (called also gyroresonance emission) is observed, while various types of transient anisotropic electron distribution functions in the active corona generate electromagnetic emission at centimetric and longer wavelengths via collective processes such as beam-plasma or loss-cone instabilities.

2.2 Magnetic Fields and the Structure of the Solar Atmosphere

Due to magnetic fields generated by a dynamo mechanism in the *convection zone* underneath the photosphere, the atmospheric structure, especially in the corona, is far from being spherically symmetric. Figure 2 shows views of different temperature regimes of the atmosphere through images at different wavelengths taken on a day of weak activity ("quiet" atmosphere, Fig. 2.a) and on a day when two active regions are present in the eastern hemisphere (left half of the images in Fig. 2.b, zoom on one of the active regions in Fig. 2.c).

Zeeman effect measurements in photospheric lines provide maps of the line-of-sight component of the magnetic field (top row) where active regions appear as magnetic field concentrations with a bipolar or a more complex multipolar configuration. Photospheric continuum emission (second row from top) shows sunspots, which are darker (cooler) than the average photosphere, and surrounding faculae, which are brighter (hotter) than the quiet photosphere at a given optical depth. Chromospheric lines (central row) show bright plages above regions of strong photospheric fields. The chromospheric lines also reveal structure outside active regions, such as the dark filaments (Fig. 2.a, near the south-eastern limb; Fig. 8a for a detailed view of another filament), which are concentrations of cool matter ($\sim$7000 K) within the hot ambient corona. When seen at the limb, these structures are bright with respect to the dark sky, and are called prominences for historical reasons (e.g. the gray feature embedded within the background corona at an angle ~ 36 deg clockwise from top in Fig. 3).

X-ray (Fig. 2.a, second panel from bottom) and radio emission (bottom) of the quiet corona trace the thermal plasma, including the extended regions of low brightness (low electron density and temperature) at the poles and on the disk: coronal holes. These features have no evident counterpart in the underlying atmosphere. They overly photospheric regions with weak unipolar magnetic fields, and the coronal field lines are open towards interplanetary space. Coronal holes are the source of the fast solar wind. The corona of active regions consists of hot and dense plasma loops giving bright X-ray emission (Fig. 2.b, c). In these regions the plasma delineates predominantly (but not exclusively) closed magnetic field structures. The numerous bright points found in EUV- and X-ray images all over the Sun (Fig. 2.a) overly small bipolar magnetic field patterns in the photosphere outside active regions.

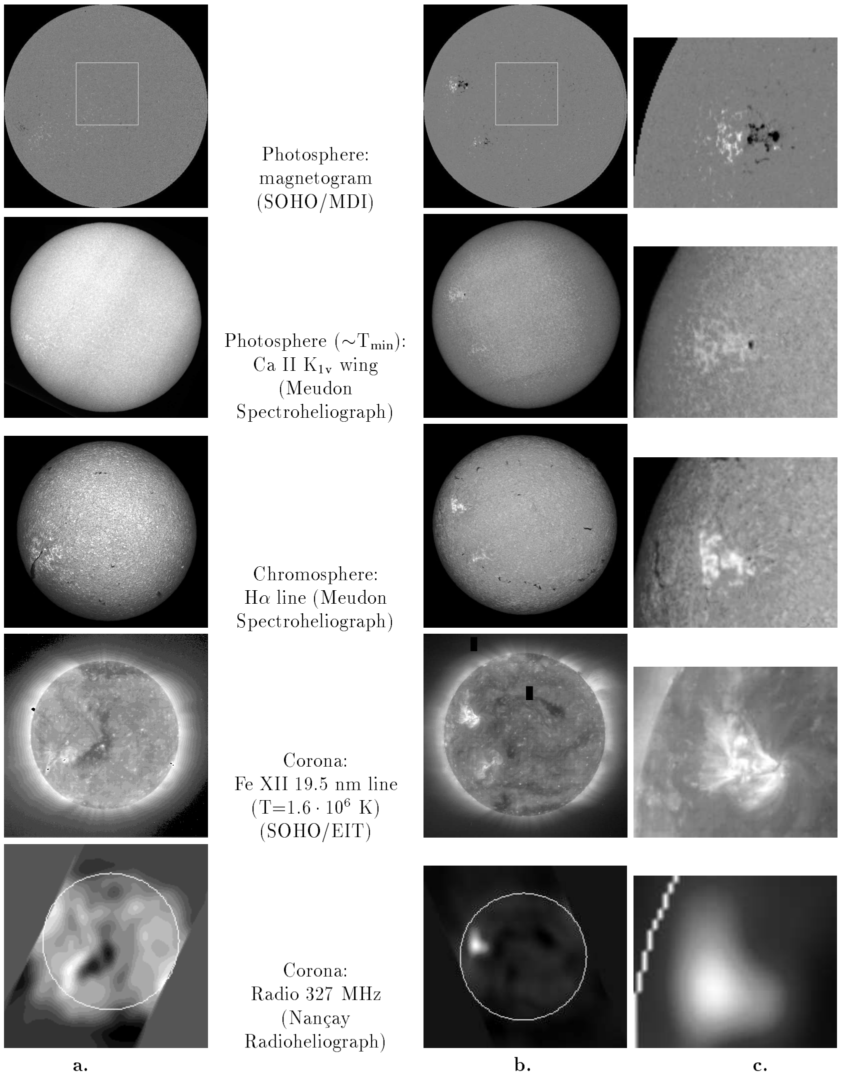

Fig. 2. Views of the solar atmosphere at different wavelengths, during a quiet period (**a**) and in the presence of active regions (**b**). (**c**) is a zoom of the north-eastern (upper left) active region

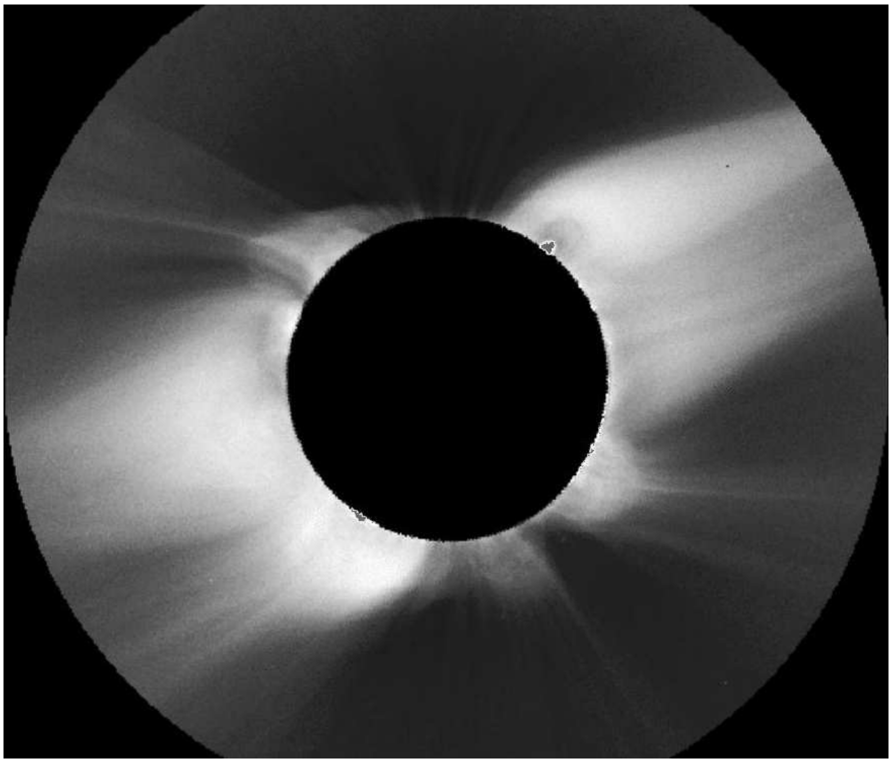

Fig. 3. Solar eclipse in white light (courtesy *High Altitude Observatory*, Boulder)

At decimetric and longer wavelengths suprathermal electrons accelerated in active regions provide a bright emission through collective processes ("noise storms") that outshine emission of the hot thermal plasma by one to two orders of magnitude (Fig. 2.b, c, bottom).

At heights above (1–2) $R_\odot$ above the photosphere the plasma structures seen in white light indicate that the magnetic field is mostly open. The most prominent extended structures on eclipse photographs (e.g. Fig. 3) are the coronal streamers. Their shape suggests that a closed magnetic field configuration at low heights, covering a large surface on the Sun, narrows with increasing altitude, and is eventually torn open by the outward streaming (slow) solar wind. Closer inspection of eclipse observations and of measurements using the signals of artificial or cosmic radio sources traveling through the outer regions of a streamer show numerous, more or less radially oriented, narrow structures which have been interpreted as multiple current sheets on top of the closed magnetic structure at the base of the streamer (Woo et al. 1995).

The atmospheric structures identified in these figures are quasi-steady in that they keep a similar shape for several days or weeks. But a permanent energy input is required to maintain the hot plasma and the nonthermal electron populations.

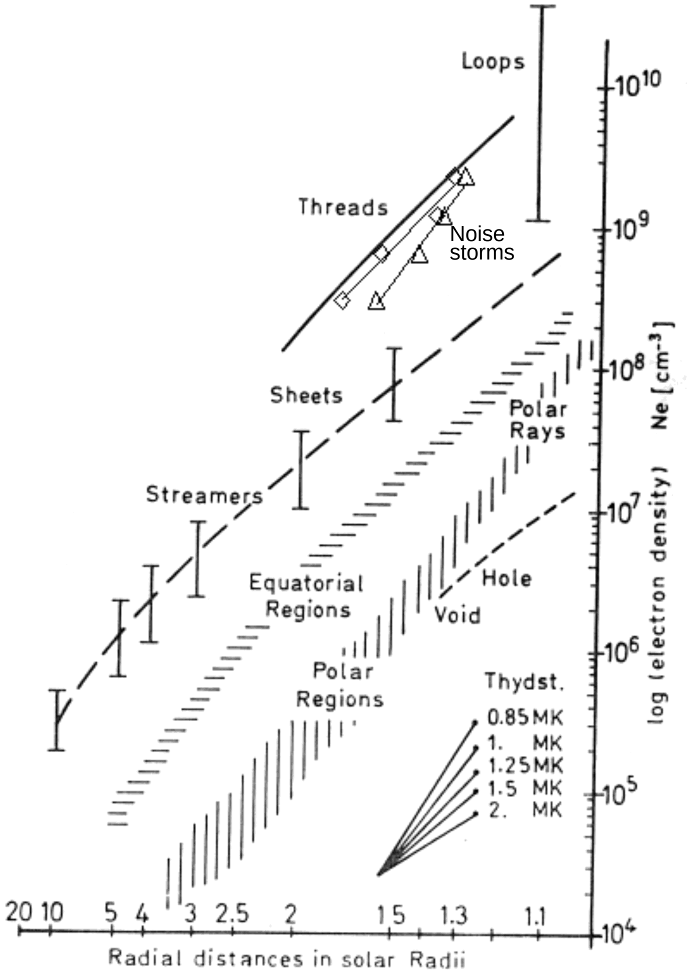

Fig. 4. Density vs. height profiles in different coronal structures (inferred from white light observations, Koutchmy 1994) and from noise storm observations with the *Nançay Radioheliograph*

Coronal Electron Density The analysis of images in coronal emission lines (visible light, EUV, X) shows that the low corona has a heterogeneous (electron) temperature structure, ranging from the vicinity of 10^6 K to $\sim 7 \cdot$

10^6 K. Plasmas of different temperatures, seen in different wavelength ranges, may be confined in different loop structures. Furthermore the legs of identified loops are usually cooler than their summits. Commonly quoted values of the electron density at the top of soft X-ray loops in active regions are in the range $(3-13)\cdot 10^9$ cm^{-3} (e.g. Yoshida and Tsuneta 1996), and similar values are inferred from white-light observations (Fig. 4). These are lower limits, due to the assumption that the plasma fills a loop whose dimension along the line of sight is comparable to the observed width.

Ion temperatures can be derived from the widths of EUV emission lines, provided that competing broadening effects such as unresolved small-scale motions of the plasma in the source region can be corrected for. Recent SoHO analyses of coronal holes suggest that ion temperatures are considerably higher than electron temperatures (Tu et al. 1998; Wilhelm et al. 1998; David et al. 1998) - e.g. $T_i \simeq (1-5)\cdot 10^6$ K for Ne ions as opposed to $T_e < 10^6$ K, and that different ions have different temperatures. The decreasing role of collisions seems to become noticeable in the low-density plasma of coronal holes, even at altitudes as low as a fraction of a solar radius. The large ratio of ion-to-electron temperature in coronal holes is similar to the results of in situ measurements in fast solar wind streams by Helios at 0.3 AU, while in slow solar wind streams the electron temperature seems slightly higher than the proton temperature (Schwenn 1990).

Part of the coronal white-light emission is due to Thomson scattering of photospheric light by the coronal electrons. Its intensity measures the integrated electron density along the line of sight, and can be used to infer the electron density in large-scale coronal structures. Using eclipse observations and assumptions on the dimension of the sources along the line of sight, Koutchmy (1994) derived the electron density distributions of Fig. 4 for various coronal structures. Other density measurements for the quiet Sun and coronal holes from both white-light continuum and EUV lines give curves similar to those of the equatorial and polar regions of the quiet Sun in Fig. 4 (Withbroe 1988; first SoHO results in ESA SP-404). The plot represents log n_e as a function of $R_\odot/r$, the inverse of the heliocentric distance in units of the solar radius. In this representation the barometric isothermal density law in an unmagnetized plasma

$$n_e(r) = n_e(R_\odot)\exp[-\frac{R_\odot}{H_\odot}(1-\frac{R_\odot}{r})]$$

is a straight line. Here $H_\odot = \frac{kT}{\mu m_p g_\odot}$ is the density scale height, k Boltzmann's constant, $g_\odot$ the gravitational acceleration at the solar surface, m_p the proton rest mass, $\mu = 0.6$ the mean molecular weight. $n_e(R_\odot)$ is the reference density at the base of the corona.

The local electron density can in principle be inferred from the measurement of positions of dm/m-wave noise storms (cf. Fig. 2.b,c bottom panels) without the need to inverse the line-of-sight integration. The radiation is generated close to the plasma frequency. The open diamonds and triangles labeled 'Noise storms' in Fig. 4 were derived from the position measurements at four frequencies of the centroids of two noise storms at the solar limb (data from the *Nançay Radioheliograph*). The straight lines give least-squares fits to the two data sets. The density profiles are quite similar to those inferred from the visible-light-observations in dense coronal structures.

The empirical density profiles at heliocentric distances $< 2\ \mathrm{R}_\odot$ have slopes close to those predicted by the isothermal hydrostatic model with $T = (1-2) \cdot 10^6$ K, as indicated for different temperatures by the bundle of straight line segments in the lower right corner of Fig. 4. The absolute densities differ by up to three orders of magnitude between different coronal structures. While the agreement with a static model is not a surprise, given that the flow speeds at low altitudes are largely subsonic, it must be kept in mind that the measured densities are average values, due to the line-of-sight integration of the optical data and to the smearing out of the radio structures by coronal scattering and the antenna beam.

Magnetic Field Quantitative information on magnetic fields is mostly derived from Zeeman or Hanle effect measurements of spectral lines from rather cool plasmas, in the photosphere or in prominences. Coronal emission lines are too broad to allow Zeeman effect measurements. It is general use to infer the topology of the coronal magnetic field from the extrapolation of the measured photospheric field, using a current-free or a force-free model, and to constrain the models by the observed plasma structure. Direct determinations of the coronal magnetic field are only possible through the measurements of the circular polarization of thermal free-free emission at centimetric wavelengths and from observations of centimetric cyclotron emission in the coronal part of active regions above sunspots. The latter technique reveals that magnetic fields above 0.1 T exist in the $T \geq 10^6$ K plasma at several 10^3 km above sunspots in the photosphere (cf. reviews by Alissandrakis 1994; Klein 1992).

The magnetic field strength in the high corona, at altitudes between 2 and 9 $\mathrm{R}_\odot$ above the photosphere, can be measured through the Faraday rotation of a linearly polarized signal from interplanetary spacecraft or from cosmic radio sources on its way through the corona (review by Bird and Edenhofer 1990). Measurements during weak solar activity show the field strength to decrease as the sum of an $(\frac{r}{R_\odot})^{-3}$ and an $(\frac{r}{R_\odot})^{-2}$ term at heights $> 2\ \mathrm{R}_\odot$ above the photosphere. This also fits in situ measurements at 0.3 AU.

Plasma Parameters in Solar Atmospheric Structures A summary of typical plasma parameters in different atmospheric structures, inferred from observations and semi-empirical modelling, is given in Table 1. Since the temperature (T), density (of thermal electrons, n_e, and neutral hydrogen atoms, n_H) and magnetic field values (B) are derived from imaging observations,

Table 1. Typical averaged parameters of solar atmospheric structures

	T [K]	n_e [m^{-3}]	n_H [m^{-3}]	B[T]
Photosphere [a]				
Bottom	6500	$8 \cdot 10^{19}$	10^{23}	-
Sunspot	4000	$5 \cdot 10^{18}$	$4 \cdot 10^{23}$ [b]	0.3
Temp. min	4400	$3 \cdot 10^{17}$	$2 \cdot 10^{21}$	
Chromosphere				
Quiet[c]	10^4	$4 \cdot 10^{16}$	$5 \cdot 10^{16}$	$3 \cdot 10^{-3}$
Plage[d]	10^4	$3 \cdot 10^{17}$	$4 \cdot 10^{17}$	$3 \cdot 10^{-2}$
Corona				
Hole	$\leq 10^6$	10^{13}	-	10^{-4}
Active region	$4 \cdot 10^6$	10^{16}	-	10^{-2}
Quiet	$2 \cdot 10^6$	10^{14}	-	10^{-3}
Prominence	7000	10^{16}	10^{17}	10^{-3}

	$f_{\rm pe}$ [s^{-1}]	$f_{\rm ce}$ [s^{-1}]	$\nu_{\rm ep}$ [s^{-1}]	$\nu_{\rm en}$ [s^{-1}]	$\sigma[(\Omega{\rm m})^{-1}]$
Photosphere					
Bottom	$8 \cdot 10^{10}$	-	-	10^{10}	90
Sunspot	$2 \cdot 10^{10}$	$9 \cdot 10^9$	-	$3 \cdot 10^{10}$	2
Temp. min	$5 \cdot 10^9$		-	10^8	25
Chromosphere					
Quiet	$2 \cdot 10^9$	$9 \cdot 10^7$	10^6	$4 \cdot 10^3$	10^3
Plage	$5 \cdot 10^9$	$9 \cdot 10^8$	10^7	$3 \cdot 10^4$	10^3
Corona					
Hole	$3 \cdot 10^7$	$3 \cdot 10^6$	1	-	$7 \cdot 10^5$
Active region	$9 \cdot 10^8$	$3 \cdot 10^8$	10^2	-	$6 \cdot 10^6$
Quiet	$9 \cdot 10^7$	$3 \cdot 10^7$	3	-	$2 \cdot 10^6$
Prominence	$1 \cdot 10^9$	$3 \cdot 10^7$	10^6	$8 \cdot 10^3$	$8 \cdot 10^2$

[a] cf. Maltby et al. 1986, ApJ 306, 284
[b] Denser than the photospheric bottom because observed at a lower height
[c] cf. Vernazza et al. 1981, ApJS 45, 635
[d] cf. Lemaire et al. 1981, A&A 103, 160

they are average quantities affected by the integration along and perpendicular to the line of sight. The magnetic field values cited for the corona are consistent with present knowledge, but are in general not directly measurable (with the exception of prominences: see Sec. 5.2). $f_{\rm pe}$ and $f_{\rm ce}$ are the electron plasma frequency and the electron cyclotron frequency, respectively. Characteristic frequencies of momentum exchange are given for collisions of electrons with protons (ν_{ep}) and with neutral hydrogen (ν_{en}; after Melrose and Khan 1989). The indicated electric conductivity σ is the minimum value of those inferred from collisions of electrons with neutrals (photosphere; cf. Stix 1991, ch. 8.1.2) and with protons. Photospheric electrons are supplied by heavy atoms with low ionisation potential, while hydrogen is neutral. This is why no electron-proton collision frequency is listed for the photosphere.

2.3 Subphotospheric Motions as Drivers of Solar Activity

The evolution of the plasma structures and the measurement of photospheric magnetic fields show that the plasma β decreases with increasing height in the solar atmosphere, and increases again at heights of solar wind acceleration. The photosphere is a high-β plasma, where the pressure of the convected gas concentrates magnetic fields in individual flux tubes. Sunspots are the greatest and most conspicuous of them, but flux tubes of smaller spatial scale form a network in the photosphere on the borders of convective cells with a typical size of 30,000 km (supergranulation cells; $B \geq 0.1$ T). It seems that with increasing spatial resolution more concentrated magnetic fields become visible in the "quiet" photosphere.

Material motions observed in the photosphere reflect processes in the underlying convective zone. The density scale height in the convective zone below the photosphere goes from ≈ 100 Mm at the bottom to 0.2 Mm at the top. Compared to the height of the convective zone, this implies a density ratio between the bottom and top of $\approx 10^6$. This strong density stratification (coupled to mass conservation) creates a strong asymmetry between upward and downward motions: the ascending plasma must rapidly expand, then it must overturn within a density scale height while the descending plasma must rapidly contract and continue to fall down, becoming more concentrated and more dense. It implies that the convective zone has gentle ascending motions and strong concentrated downflows (just the opposite to the hot ascending plumes in the earth's upper mantle !). Convective motions concentrate magnetic fields in individual flux tubes, part of which may become buoyantly unstable and rise through the photosphere. The emergence of magnetic flux above the photosphere is visualized e.g. by "arch filament systems" (AFS). They are formed by several dark arches with a blue-shifted summit and red-shifted legs (e.g. Chou and Zirin 1988; Alissandrakis et al. 1990, Mein et al. 1996). The observed Doppler velocities are direct signatures of emerging magnetic loops with dense plasma leakage in the legs.

The coupling of the magnetic field in the atmosphere with material motions in and below the photosphere is the basic process driving the transport of energy into the corona. Motional electric fields for typical photospheric (horizontal) speeds of 0.5 km s^{-1} and magnetic fields of $\sim$100 G provide a Poynting flux of $5 \cdot 10^4$ Wm^{-2} (Einaudi and Velli 1994). The energy loss of the corona ranges from several 10^2 Wm^{-2} in a coronal hole to 10^4 Wm^{-2} in an active region. Therefore the Poynting flux is sufficient to explain coronal heating and solar wind acceleration. However, the power supplied to the active region corona (typical photospheric surface 10^{15} m^2) is 10^{20} W, which is not sufficient to power a conspicuous flare. A flare requires energy storage during up to a day, presumably in the magnetic field configuration.

3 Why an MHD description of the corona ?

The convective zone governs the physics in the corona both by successive emergences of magnetic flux and by imposing horizontal photospheric motions. The coronal magnetic field and plasma are forced to evolve according to the time-dependent boundary conditions imposed at the photospheric level by the convective zone. This boundary driving is however slow at the bottom of the corona (few km.s^{-1}) compared to the sound and Alfvén speed (see Table 2) and it is fundamentally different from the super Alfvénic driving ($M_A \approx 10$) of the terrestrial magnetosphere by the solar wind. The subphotospheric driving induces a quasistatic evolution of the coronal magnetic field which is interrupted from time to time by dynamical events. Part of the free-energy is either dissipated directly or stored for a short duration and released frequently in small events giving an "average" coronal heating. The other part of the free-energy is stored on a longer time (hours to days) and it is liberated only when a global instability of the magnetic configuration occurs; it leads to flares and CMEs.

A second major difference between the terrestrial magnetosphere and the solar corona is the plasma densities; they imply a collisionless plasma for the magnetosphere while in the corona the frequency of collisions is much higher than the bounce frequency (see Table 2). This permits to use MHD equations for analysing the large-scale magnetic configurations in the corona and their evolution. A third difference is the importance of the magnetic field in the physics involved: while the low corona is fully dominated by the magnetic field (low β plasma, see Table 2) particle pressure cannot always be neglected in the magnetosphere (see e.g. Fontaine 1998).

On top of these three main physical differences is the weight of the observing technics: localized measurements of particle distribution functions, fields and currents versus remote sensing imaging and spectrographic observations measuring density, velocity and magnetic field averaged over the instrumental response function. The MHD description of the corona attempts to understand the evolution of magnetic structures on the large spatial scales accessi-

Table 2. Order of magnitude for the physical parameters in the low solar corona. The numerical values (third column) are given for a temperature $T = 10^6$ K, a density $N = 10^{15}$ m^{-3}, a magnetic field $B = 10^{-2}$ T (and $\ln \Lambda = 20$) which are typical for the low corona. Variation from these values can be easily computed by using the parameter dependence reported in the fourth column with the quantities T, N, B normalized to the above values. (From Chen 1984, NRL Memorandum Report 1977; Priest 1982; Stix 1991)

parameter	symbol	typical value	dependence
Lengths			
active region	L_{AR}	10^8 m	
scale height	H_g	$5 \cdot 10^7$ m	T
supergranule	L_{SG}	$3 \cdot 10^7$ m	
sunspot	L_{SS}	10^7 m	
granule	L_G	10^6 m	
Collision mean free path	$\lambda_{ee} \approx \lambda_{ep} \approx \lambda_{pp}$	$2 \cdot 10^5$ m	T^2/N
Plasma skin depth		$2 \cdot 10^{-1}$ m	${N_e}^{-1/2}$
Proton gyro radius	r_p	10^{-1} m	$\sqrt{T_p}/B$
Debye length	λ_D	$2 \cdot 10^{-3}$ m	$\sqrt{T_e/N_e}$
Electron gyro radius	r_e	$2 \cdot 10^{-3}$ m	$\sqrt{T_e}/B$
Times			
Solar cycle		22 years	
active regions, filaments		10^7 s	
CMEs		10^5 s	
Flares: Main phase		10^4 s	
Impulsive phase		$3 \cdot 10^2$ s	
Hard X-rays spikes		10^{-1} s	
Radio spikes		10^{-2} s	
Frequencies			
Electron gyrofrequency	f_{ce}	$3 \cdot 10^8$ s^{-1}	B
Plasma frequency	f_{pe}	$3 \cdot 10^8$ s^{-1}	$\sqrt{N_e}$
Proton gyrofrequency	f_{cp}	$2 \cdot 10^5$ s^{-1}	B
Electron-electron collision rate	ν_{ee}	50 s^{-1}	$N_e {T_e}^{-3/2}$
Electron-proton collision rate	ν_{ep}	30 s^{-1}	$N_e {T_e}^{-3/2}$
Proton-proton collision rate	ν_{pp}	1 s^{-1}	$N_p {T_p}^{-3/2}$
Bounce frequency for electron	V_{Te}/L_{AR}	$4 \cdot 10^{-2}$ s^{-1}	$\sqrt{T_e}$
Bounce frequency for proton	V_{Tp}/L_{AR}	10^{-3} s^{-1}	$\sqrt{T_p}$

Table 2. Continued

parameter	symbol	typical value	dependance
Velocities			
particle beams		up to $3 \cdot 10^5$ km s^{-1}	
solar wind		≈ 700 km s^{-1}	
jets		few 100 km s^{-1}	
quiescent coronal evolution		$1 - 10$ km s^{-1}	
photospheric motions		$0.1 - 1$ km s^{-1}	
Electron thermal speed	V_{Te}	$4 \cdot 10^3$ km s^{-1}	$\sqrt{T_e}$
Alfven speed	V_A	10^3 km s^{-1}	$B/\sqrt{N}$
Sound speed	C_s	$2 \cdot 10^2$ km s^{-1}	$\sqrt{T}$
Proton thermal speed	V_{Tp}	10^2 km s^{-1}	$\sqrt{T_p}$
Plasma parameters			
Plasma parameter	$N_e \lambda_D^3$	10^7	${T_e}^{3/2} {N_e}^{-1/2}$
Plasma beta	β	$4 \cdot 10^{-4}$	$NB^{-2}T$
Magnetic diffusivity	η	1 m^2 s^{-1}	$T^{-3/2}$

ble to telescopes, and to infer where the macroscopic approach breaks down, i.e. where energy will eventually be released. The basic boundary conditions are magnetic fields and flow fields, $\boldsymbol{B}$ and $\boldsymbol{v}$, measured at the photospheric level. Magnetospheric diagnostics, on the other hand, provide local parameters from which the global configuration must be inferred. The difficulty to do this adequately with a kinetic approach is such that even in the magnetosphere MHD is frequently used in a global approach (e.g. Birn et al. 1996; Hesse et al. 1997). Obviously, in both fields kinetic theory, or even more a particle approach is needed when the detailed process of energy release is to be analyzed.

Even when the object of the study is the global understanding of the physical system, the "acroscopic" equations used, as well as the concepts behind, are different. The long standing controversy on whether one should mainly use MHD with $\boldsymbol{B}$ and $\boldsymbol{v}$ for the primary variables, or rather use $\boldsymbol{E}$ and $\boldsymbol{j}$ leads to many misunderstandings between the two communities. They are still well alive as the recent debate between Parker (1996, 1997) and Heikkila (1997) shows.

MHD equations express the conservation of fundamental macroscopic quantities (mass, impulsion and energy). They are derived from the Boltzmann equation by integrating over the velocity space, so there is some lost information (see e.g. Parker 1994; Heyvaerts 1998). In the study of solar atmospheric structures some simplifying approximations are well justified: nonrelativistic regime, fluid approach (enough particles or dominant magnetic field), evolution time much longer than the cyclotron period of particles, absence of large-scale field-aligned potential drops. Some are more questionable, for example, an evolution time much larger than the thermalisation time of the particles. Moreover coefficients (like viscosity and resistivity) and the equation of state need to be specified in MHD equations. They are derived from kinetic theory in "ideal" cases (e.g. local thermal equilibrium) which are not necessarily valid in the applications. The relatively small mean free path of particles compared to global sizes (see Table 2) means that the Coulomb collisions are so frequent in the low corona that MHD may still be a good first approximation to study the processes involved.

One of the most troublesome parts of MHD may be the treatment of the relationship between current density and electric field. This is done through a generalised Ohm's law derived basically from the momentum equation of electrons. In the study of equilibrium configurations and their slow, quasi-static evolution in the coronal low β plasma an order of magnitude estimation of the terms leads usually to simplify this equation to retain only the resistive term ($\boldsymbol{j} = \sigma \boldsymbol{E}$, see e.g. Priest 1982). This is further justified by Parker (1994, Chapter 2) who show that only some terms of the generalised Ohm's law have an effect on the magnetic field evolution and that such terms are usually negligible. In most analyses, including numerical simulations, the electrical conductivity reduces to a scalar. This is clearly an oversimplification which is imposed by the limited resources of present computers. Even using super-computers, the scalar conductivity used needs to be reduced by many orders of magnitude compared to the estimated coronal one if one want to study a global magnetic configuration. This may look very far from coronal physics, but it is less than one might think. There are several studies on magnetic reconnection and MHD turbulence which show that the energy release depends only weakly (logarithmic dependance) on the magnitude of the dissipative coefficients (see e.g. Biskamp 1993). In fact, with lower dissipation coefficients, the energy simply cascades to smaller scales, where it is finally dissipated. The input of the energy at large scales is basically fixed by the global evolution of the system, e.g. a large scale instability.

There is an important restricted version of the MHD equations, so-called ideal MHD, which is free of the problems described above and can still give several hints on the magnetic-field physics. In ideal MHD both viscosity and resistivity are set to zero (or more precisely both Reynolds numbers are infinite). In the corona, one can even get a step further and neglect the plasma pressure (so no state equation is needed). This is a useful over-simplification because of the low β plasma and the high Reynolds numbers in the low corona. This simplified version of MHD is self-consistent (no need to define any plasma coefficient). This framework provides very valuable insight in how the whole magnetic system evolves. In particular it permits to understand how the energy is stored, when the system becomes globally unstable, so when the stored energy can be released. Moreover, it shows also where current sheets (or layers) are formed, so the spatial locations where magnetic energy can be efficiently transformed (by reconnection). The results can be directly tested with observations (Section 4).

The ideal MHD approach shows also its own limits: the MHD equations are obviously invalid at the current layers. There, locally, a kinetic approach is required, but it needs to be coupled to the global configuration described by MHD, because both the spatial location and the intensity of the current layers are determined by the global evolution of the system. The resistive MHD can provide the global energy budget (see above), but cannot describe the energy release itself, for example the energization of particle beams. So for a full understanding of the processes both approaches, coupled together, are needed; this is a huge challenge ! At present there are still many unresolved questions on storage and sudden release of the magnetic energy, that MHD equations, even simplified ones, will still be of great help to understand the various solar observations.

4 Magnetic Energy Conversion in the Solar Atmosphere

The transformation of magnetic energy takes various forms in the solar atmosphere ranging from the de-stabilisation and ejection of a fraction of the corona down to the very small events implied in quasi-continuous coronal heating. Magnetic reconnection is thought generally to be at the heart of the energy conversion processes. In the following we emphasize the overall topology of the coronal magnetic field, as a basic concept to understand where energy could be released in a highly conductive medium. We do not discuss how energy is released. The relevant mechanisms involve sub-telescopic scales and non-MHD treatments, but they act in a macroscopic environment which can be realistically described by the MHD approach (cf. also Einaudi 1998).

4.1 Magnetic Topology

Under typical coronal conditions the magnetic field is nearly force-free and frozen into the plasma almost everywhere in active regions on the Sun. An exception is separatrices which are magnetic surfaces where the magnetic field line linkage is discontinuous (see Fig. 5). A particularly important location for reconnection (in a classical view) is the intersection of two separatrices, called a separator. Most of the reconnection theories locate the energy release at or in the close vicinity of a separator, because a current sheet forms generally at a separator when the magnetic configuration evolves. The simplest example

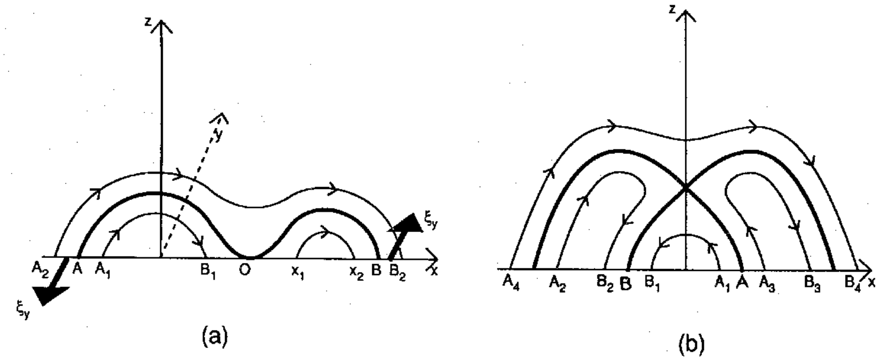

Fig. 5. Basic magnetic topology in a quadrupolar configuration. In (**a**) the separatrix (*thick line*) is tangent to the boundary at the point named "O" (it is a "bald patch"), while in (**b**) two separatrices intercept at an X point. In both cases the connectivity of field lines (*thin lines*) is discontinuous at the separatrices (as emphasis by the labeling of the foot-point of field lines). Shearing photospheric motions (*thick arrows*) induce the formation of a current sheet all along the separatrix in (**a**) (resp. separatrices in (**b**)). (From Vekstein and Priest 1992)

is a 2-D magnetic configuration with a neutral X-point (which is a particular case of separator) as in Fig. 5b. Adding a third perpendicular component of the field, which is invariant in this perpendicular direction (so-called 2.5-D configurations), yields a new possibility for the current sheet formation. They can be formed now along the whole separatrices even when smooth shearing flows are present at the photospheric boundary (e.g. Zwingmann et al. 1985). This may occur in two distinct cases (see Fig. 5). Firstly when there is an X-point in the poloidal field (Low and Wolfson 1988; Finn and Lau 1991; Vekstein and Priest 1992). Secondly when there are field lines tangent to the photospheric boundary (Wolfson 1989; Low 1992; Vekstein et al., 1992). These locations of the photospheric inversion line where field lines are tangential and upward curved are called for brevity "bald patches" (BPs) by Titov et al. (1993).

In 3-D generic cases the separatrices generalize directly the above two classes. Separatrices are formed by field lines, which thread either null points or bald patches. Current sheets are thought to form along the separatrices when arbitrary motions are imposed at the photospheric plane (e.g. Aly 1990; Lau 1993). The generalization of 2-D null point to 3-D has received most of the attention because it defines a clear topology, both locally around one null and globally (the separator being the field line linking two nulls).

From observations, several flares have magnetic nulls in their reconstructed magnetic configuration but the relation of magnetic nulls with flares is not systematic (Démoulin et al. 1994). This was a first motivation for the generalization of separatrices to quasi-separatrix layers (QSLs). A second motivation, more theoretical, is summarized in the next paragraph. The notion of QSLs is related to some recent developments of 3-D magnetic reconnection theory. QSLs are the generalization of separatrices to magnetic configurations with a non-zero magnetic field strength everywhere in a region (Priest and Démoulin 1995). By definition the magnetic connectivity in QSLs enormously changes with slight variations of position of the field line footpoints. QSLs play a similar role as true separatrices, i.e. QSLs as well as separatrices are responsible for generating strong current layers and magnetic reconnection is expected even in plasma with a high magnetic Reynolds number (Démoulin et al. 1996a).

The need to generalize the concept of separatrices to QSLs is illustrated here with a particular example. Let's consider a quadrupolar magnetic configuration invariant in one direction, called y, like in Fig. 5b. The intersecting separatrices define four cells of connectivity. However, when the magnetic configuration has a finite extension in the y direction, there are no longer separatrices, in the cases with no bald patches and with a non-vanishing B_y component (so no magnetic null point). The structural instability of separatrices, when going from 2.5-D to 3-D, was first point out by Schindler et al. (1988) in the case of twisted magnetic configurations (with applications to the magnetospheric tail). However this structural instability is no longer present when the notion of separatrices is generalized to those of QSLs (Démoulin et al. 1996b).

4.2 Large Scale Magnetic Restructuring: Coronal Mass Ejections

Coronal Mass Ejections (CMEs) have been extensively observed in white light coronagraphs on Skylab, SOLWIND, SMM (Solar Maximum Mission) and presently with SOHO. Solar wind and CMEs are the two main hydromagnetic phenomena which eject plasma and magnetic fields out of the sun. A CME destabilizes a large part of the corona: its extension is usually of the order of one solar radius when it is first discernible in coronograph images (and its size in the interplanetary medium increases nearly linearly with distance from the sun). The ejected mass in one CME is typically of the order of $\approx 10^{12}$ kg, with a kinetic and gravitational energy of $\approx 10^{24} - 10^{25}$ J. The velocities are typically a few hundred km.s^{-1}up to one thousand km.s^{-1}(this upper value has the magnitude of the Alfvén velocity). While a flare is often observed in conjunction with a CME, it seems to start after the time when the backward extrapolation of the CME trajectory intersects the photosphere. The energy released in the flare is variable, but can be of the same order as the kinetic or potential energy of the CME. The relative timing of CMEs and flares shows that the mass ejection is not the consequence of the explosive energy release during the flare, but constitute a specific manifestation of coronal magnetic field de-stabilisation.

A long standing question during the past thirty years dealt with the possibility to open a magnetic configuration. On one hand, the coronal plasma observations seem to indicate such opening, on the other hand the models have difficulties to explain such phenomena. The coronal magnetic Reynolds number being huge (10^{12}–10^{14}) on large scales, an ideal instability is more likely to drive the process initially. This problem was difficult to solve and it is only recently that a consensus has grown. A common result to all present numerical simulations is that the stored energy in a force-free field cannot exceed the energy of the associated open field (with the same photospheric magnetic-flux distribution; this provides a numerical validation to the conjecture of Aly (1991) and Sturrock (1991).

An important step in the analysis of the problem has been to consider axisymmetric magnetic configurations around a sphere rather than a cartesian geometry invariant by translation. The main difference is in the property of the open-field: it has a finite energy in the axisymmetric geometry while its energy is infinite in the cartesian geometry (even per unit of length in the invariant direction). Then photospheric shearing motions can drive the system to the open state in a finite time (compared to an infinite time in the cartesian 2.5-D geometry). This has been shown both by analytical (Lynden-Bell and Boily 1994; Aly 1995; Sturrock et al. 1995; Wolfson et al. 1996) and by numerical (Mikić and Linker 1994) approaches. The inclusion of resistivity allows the formation and ejection of a twisted flux tube. The actual precise amount of resistivity seems to play a minor role (see Section 3). The inclusion of solar wind makes the eruption more energetic (Linker and Mikić 1995). These works represent an important step compared to the cartesian case. In particular the field opens after a finite time, but this time, around 30 days with differential rotation, is too long compared to the observed rate of CMEs (about 1 per day).

Only recently has the analysis of the full 3-D problem become possible, due to the development of powerful numerical techniques and computers. Slow photospheric twisting motions applied to a simple bipolar field force the configuration to expand upward, initially at a speed lower than the driving speed, but later much faster (a non negligible fraction of the Alfvén speed; Amari et al. 1996). Because the twisting motions have been applied only to part of the photospheric field, the configuration tends to a partially open field in a finite time. The amount of twist needed, of about one turn, is more compatible with the observations than in the previous axisymmetric configurations. Finally, the full 3-D system has more freedom than the axisymmetric one: in particular the twisted flux tube can push the untwisted field lines aside, while in an axisymmetric system they would be forced to become open too. This effect facilitates the partial opening of the field. This opening phenomenon has been found to occur in various configurations (Amari et al. 1997a).

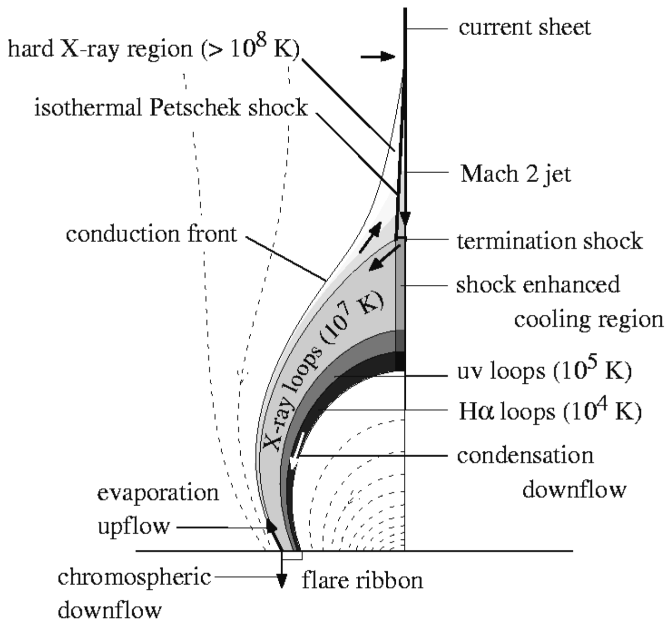

Fig. 6. Schematic diagram representing the characteristics of supermagnetosonic regime in flares together with the observational consequences. This regime is most likely to occur in the early phase of the flare when reconnecting fields are strong. Solid lines indicate boundaries between various plasma regions, while dashed lines indicate magnetic field lines. Arrows represent the plasma flows. (From Forbes and Acton 1996)

4.3 Magnetic Field Evolution and Energy Dissipation During Flares

Flares are observed in the whole spectrum ranging form radio to γ-rays. There are a rich variety of magnetic configurations; models have to explain how and where magnetic energy is released in solar flares and in particular the existing link between chromospheric flare ribbons sometimes separated by more than 100 Mm. "Post" flare loops are seen to form between the flare ribbons during the development of most flares (see Schmieder 1992 for a review and Malherbe et al. 1997 for a time evolution of the phenomena) suggesting a model with reconnection (e.g. Forbes and Acton 1996; van Driel et al. 1997). Many observational studies in different wavelengths show that flares, and even less intense coronal phenomena, involve interactions between coronal magnetic structures (see e.g. Machado et al. 1988; Shimizu et al. 1994; Hanaoka 1995; van Driel-Gesztelyi et al. 1996). Figure 6 gives a summary of how the reconnection process is envisioned and how it may affect different regions of the solar atmosphere.

Fig. 7. Example of the correspondence between the flare ribbons and the trace of computed QSLs in a simple flaring region **(a)** Observational data: Off-band Hα flare kernels (hatched regions) and longitudinal photospheric field (positive and negative values are drawn with solid and dashed lines respectively) **(b)** Trace of the QSLs (thick lines) and regions where the vertical current density is greater than 10 mA m^{-2}. The coronal links between Hα brightenings are given by four kinds of field lines (the Hα kernel d is linked to local magnetic connections which are not represented). **(c,d)** Perspective view of Fig. 7b showing the coronal linkage at the borders of QSLs with field lines drawn as surfaces. (From Démoulin et al. 1997)

Since the instantaneous transport of energy from the convective region and the photosphere is not sufficient to power a flare, energy storage is a necessary ingredient of flare models. For example, it has been argued that current sheets can store enough magnetic energy to power a flare (Somov 1992 and references therein). At some point in the evolution, this current sheet becomes unstable and turbulence develops increasing the plasma resistivity. Then, the stored energy is rapidly released as a flare (e.g. Heyvaerts et al. 1977). It has instead been argued that reconnection tends to occur at a rate imposed by the evolution of the large-scale magnetic field (e.g. Priest and Forbes 1992). In this latter case, the current in the sheet is always small and magnetic energy is instead stored in smooth field-aligned currents, such as a twisted flux tube, at a spatial scale that gives a negligible role to the resistive term (length-scale typically 1-10 Mm). In this evolution an ideal instability or non-equilibrium occurs forcing reconnection to take place at the separator (e.g. Priest and Forbes 1990). Another possibility is that the field-aligned currents are formed by photospheric or convective motions and then carried towards the locations of current sheets where the stored energy can be rapidly released. This list of possible solar flare models is far from being complete, but it shows instead that we still need to combine a large set of observations with adequate modeling of the magnetic field in a search about hints on the energy release process.

In order to model an observed region we need to compute the magnetic field from the photosphere to the corona. Important difficulties (linked to the presence of concentrated currents and of separatrices) are present in 3D force-free field computations using observed magnetograms. Currently they are still not fully solved (Amari et al. 1997b; Mc Clymont et al. 1997). Present successful extrapolations, in terms of a good correspondence between the observed coronal plasma structures and the computed field lines, have been realized for moderate magnetic shear. This kind of configuration provides the most accurate test of flare models in terms of localization of the magnetic energy release in the computed magnetic configuration.

The role of magnetic reconnection in flares has been tested using a variety of photospheric, chromospheric and coronal observations. By analysing several flares Démoulin et al. (1997), Mandrini et al. (1997), and Schmieder et al. (1997) have shown that Hα (or UV) flare brightenings are located on the intersection of QSLs with the chromosphere and that they are connected by magnetic field lines which trace the flare loops observed in soft X-rays. QSLs are formed in a variety of observed magnetic configurations, ranging from quadrupolar regions (an example is given in Fig. 7) to bipolar ones with an "S"-shaped inversion line and even in bipolar regions with a nearly potential field and an almost straight inversion line. The first case is a direct extension to 3-D of a 2-D magnetic configuration with an X-point (as used in 2-D reconnection models), while the second and third seem at first sight closer to a simple arcade model ! There is a wide range for the thickness of QSLs. This thickness is determined by the character (bipolar or quadrupolar) of the magnetic region and by the sizes of the photospheric field concentrations; the QSL thickness can be very small, ranging from 10^6 m down to zero (in the case of separatrices). Concentrated currents have been found in the observations; they are located at the borders of the QSLs (see Démoulin et al. 1997 and references therein). Moreover, two current kernels of opposite sign, linked by coronal field lines, are usually found at the photosphere. This indicates that the energy is presumably stored in the magnetic field associated with these field-aligned currents.

The above results give some confidence on the development of 3-D magnetic reconnection involving QSLs. They show that one needs to go beyond the classical generalization to 3-D of 2-D magnetic null points and associated separatrices. Magnetic reconnection occurs in more general circumstances when small scale lengths are formed in the system by a drastic change in the field line linkage. Magnetic configurations with field lines tangential to the photospheric boundary (at bald patches) can also lead to the formation of thin current layers (section 4.1). A first observational evidence of such a case has just been found (Aulanier et al. 1998c). It points to the need for the development of 3-D reconnection models in such a case.

4.4 Bright Points

X-ray bright points (XBPs) were first observed in images obtained by a rocket-borne grazing-incidence soft X-ray telescope (van Speybrock et al. 1970) and their characteristics were analysed in detail during the Skylab mission (e.g. Golub et al. 1977). They appear as diffuse clouds of typically 20 Mm diameter with a central bright core. They are uniformly distributed over the solar surface, with about 200 being present simultaneously and 1500 being born each day. Their lifetimes vary between 2 and 48 hours, with a mean value of 8 hours, and they are located above pairs of opposite magnetic polarities observed in the photosphere outside active regions (e.g. Harvey et al. 1994). Nolte et al. (1979) observed impulsive brightenings and rapid decays in a small sample of XBPs. They suggested that the fluctuations were driven by episodic heating superimposed upon a continuous input of energy. The cause of XBP variability is not yet clear, although some results indicate that the XBP brightenings are similar to normal flares, only smaller in energy (e.g. Strong et al. 1992), and may also involve beams of nonthermal electrons (Kundu et al. 1994).

Based on Skylab results, XBPs were originally considered the primary coronal manifestation of emerging photospheric flux. However, subsequent studies gave contradictory results concerning the nature of XBPs. Martin et al. (1985) suggested that cancelling features could be associated with XBPs. On the other hand, Golub et al. (1986) found that XBPs are more likely associated with emerging than with cancelling flux. More recently Webb et al. (1993), analyzing X-ray data from rocket flights coordinated with full-disk and time-lapse magnetograms, reached the conclusion that two-thirds of XBPs lie above decaying or cancelling magnetic features. Apart from the controversy, the important point to draw from these results is that the appearance of an XBP in the corona is independent of the type of feature seen in the magnetogram, as long as it is a bipole.

Parnell et al. (1994) showed that the analysed X-ray bright loops can be interpreted as being reconnected magnetic loops (computed from a simplified photospheric magnetogram). The process is driven by approaching magnetic flux-tubes of opposite polarity (see Parnell 1998 for further explanations). An MHD simulation of Dreher et al. (1997) confirms the formation of current sheets in such configurations and the subsequent magnetic reconnection. Mandrini et al. (1996) put forward the evidence of the role of magnetic reconnection in an XBP by using a direct extrapolation of the observed photospheric magnetic field and the QSL approach. The extrapolated field lines, with photospheric footpoints on both sides of QSLs, match the observed chromospheric and coronal structures (arch filament system, XBP and faint X-ray loops). Furthermore the calculated QSL is very thin (typically less than 100 m) during the lifetime of the XBP, but becomes much thicker ($\geq 10^4$ m) after the XBP has faded. This XBP shows an example of magnetic reconnection forced by emergence and displacement of a new bipole in an old magnetic field region, a situation which is also frequent in flares.

4.5 Coronal Heating

Energy is continuously supplied to the solar corona to maintain its temperature above 10^6 K. Since the major discovery of the existence of this very hot plasma in the 1940's, several mechanisms have been proposed. Nowadays a consensus has nearly emerged on the origin of the energy (which is thought to be injected at the photosphere as a Poynting flux) and on its mediator (namely the coronal magnetic field). The way this energy is dissipated in the corona is, however, still strongly debated (see e.g. Hollweg 1990; Gómez 1990; Einaudi and Velli 1994, for reviews). Two limiting cases have been investigated in detail: the case where the excitation time is comparable or smaller than the Alfvén transit time of the coronal loops and the case where it is much larger. For the first case, a high-frequency excitation at the lower boundary, the dissipation of MHD waves by phase mixing (Heyvaerts and Priest 1983) or resonant absorption (Goossens 1991) is a prime candidate to heat the corona. For the second case, i.e. a low-frequency excitation, the formation and dissipation of thin current sheets has been proposed (Parker 1972). Because of the high magnetic Reynolds number of the corona, dissipation is very small on the typical scale lengths of the corona, and MHD turbulence is likely to be important both in the waves (e.g. Inverarity and Priest 1995) and quasi-static (e.g. Heyvaerts and Priest 1984) approaches. For example, granular and super-granular convective motions introduce perturbations on scales of ≈ 1 Mm and ≈ 30 Mm with time scales of $\approx 10^3$ and $\approx 10^5$ s, respectively. The dissipation of the perturbations on such time scales, with a classical resistivity, requires scale lengths $\approx 10^{-5}$ times smaller than the sizes of the convective cells for both types of convection (and so scale-lengths in the range 10–300 m). Clearly an efficient way to create very fine scale lengths is required.

The creation of current sheets naturally introduces fine scale-lengths in a magnetized plasma. Starting from a simple uniform field which is braided and twisted in an arbitrary way by photospheric motions, Parker (1972) argues that current sheets may be formed in ideal MHD conditions because there is, in general, no neighbouring equilibrium compatible with the imposed boundary conditions. This work stimulated a burst of research and controversy in the field (e.g. Aly 1987; Antiochos 1987; Zweibel and Li 1987; van Ballegooijen 1988; Longcope and Sudan 1992; Longcope and Strauss, 1994). Parker provided a formal example of the formation of a surface of tangential discontinuity when a layer of force-free field is locally compressed (Parker 1990), and presented a comprehensive development of the theory of the formation of discontinuities (Parker 1994).

Numerical experiments have demonstrated how quickly thin current concentrations tend to form. van Ballegooijen (1986) analysed the response of an initially uniform field to randomly phased boundary flows (modeling turbulent photospheric flows). Because of the non-linearity of the ideal MHD equations, the energy cascades to small scale lengths. van Ballegooijen (1988) showed that, even with simple boundary flows, the photospheric displacement of field-line footpoints contains fine structures with scale-lengths that become finer with time. These short scale-lengths are transferred to the coronal field and the electric-current density builds up in time. This has been confirmed by an ideal MHD simulation of Mikić et al. (1989) and by a resistive MHD simulation of Longcope and Sudan (1994) which show that current layers are formed with a thickness that decreases rapidly with time. Thin current layers are also formed during the dynamical evolution after the loss of equilibrium (Longcope and Sudan, 1992). Such non-equilibrium situations occur typically when the twist is between one and two turns (Longcope and Strauss 1994; Gómez et al. 1995).

X-ray observations show that the coronal plasma is highly inhomogeneous; this is present in the consequences of many models cited above. The spatial distribution of the heating is thought to be even more inhomogeneous than the present X-ray observations show (with a spatial resolution ≥ 0.7 Mm). Martens et al. (1985) for example have analysed a steady X-ray flaring loop-like structure and found a very hot component (T $\approx 10^7$K); by modelling the energetics of the loops, they deduced that this component is present only in a tiny fraction ($\approx 10^{-3}$) of the volume and may be formed by about 30 current layers.

Curiously, while the heating is believed to be of magnetic origin, the regions with the highest magnetic field (above sunspots) are not bright in X-rays (e.g. Sams et al. 1992; Schmieder et al. 1996). Moreover, Metcalf et al. (1994) find no correlation between the locations of bright X-ray loops and the sites of strong photospheric currents ! These observations tell us that neither the magnetic field nor the observable electric current are determining factors for the level of heating. The X-ray bright loops are rather observed around sunspots and above plages where the photospheric magnetic field is highly fragmented into thin flux tubes (see e.g. the review of Stenflo 1994). Démoulin and Priest (1997) show that such thin flux tubes imply the presence of a large number of very thin QSLs in the corona. A main parameter is the ratio between the magnetic flux located outside the flux tubes to the flux inside. The thickness of the QSLs is approximately given by the distance between neighbouring flux tubes multiplied by the ratio of fluxes to a power between two and three (depending on the density of flux tubes). They conclude that the fragmentation of the photospheric magnetic field stimulates the dissipation of magnetic energy in the corona.

Even restricting the photospheric excitation to low-frequency, there are at least five ways to form fine structures in the coronal magnetic field. Firstly, if the field topology is complex, there is current-sheet formation (see Section 4.1). Secondly, fine structures can be introduced at the boundary because the link between the velocity pattern and the footpoint displacement is strongly non-linear: well-behaved flows produce fine structures with scale-lengths decreasing exponentially with time in the footpoint displacement (van Ballegooijen 1988). Thirdly, the continuous braiding by photospheric motions of coronal field can force the magnetic system to reach a non-equilibrium (e.g. Parker 1972; Berger, 1991; Longcope and Strauss 1994). Fourthly, the intrinsic non-linearity of the MHD equations introduces a cascade of energy to fine scales (e.g. Heyvaerts and Priest 1984; Dmitruk and Gómez 1997; Georgoulis et al. 1998). And, finally, the fragmentation in photospheric flux tubes introduces a very severe mapping distortion in the field-line linkage and creates many QSLs (Démoulin and Priest 1997). In conclusion we are far from a consensus on the mechanism of coronal heating ! Moreover, while there are several ways to form fine scale-lengths, the dissipation at these scales certainly requires more than the traditional MHD treatment. The recent discovery of different electron and ion temperatures provides a new diagnostic tool to study the relevant processes.

5 Prominences as Tracers of Coronal Magnetic Field Structures

5.1 Main Characteristics

Prominences (viewed at the limb as in Fig. 3), or filaments (viewed on the disk in Fig. 8a), are elongated structures of cold material (T $\approx$ 7000 K) suspended in the hot corona (T$\approx 10^6$ K). They must be supported against gravity because their plasma is typically one hundred times denser than the coronal medium and because they extend in height over more than one hundred times the gravitational scale height of their cold plasma. Although most observations are carried out in lines of neutral atoms, the high collision rate between ions and neutrals effectively forces the neutrals to follow the ions (the relative velocity is only of a few m s^{-1} as shown by Mercier and Heyvaerts, 1977). Coronal magnetic fields are the usual explanation for prominence support. In fact the magnetic field has even a much broader impact in the physics of the prominences: it controls both the plasma dynamics (via the momentum equation) and thermodynamics (via the thermal conduction and the heating). This key role is not always recognized at its right level because the majority of observations focuses on the plasma. Furthermore, a direct evidence for importance of the magnetic-field is less compelling in prominences than in other phenomena like arch-filament systems, surges and coronal loops. Coronal loops consist basically of hot plasma which fills the magnetic flux tubes,

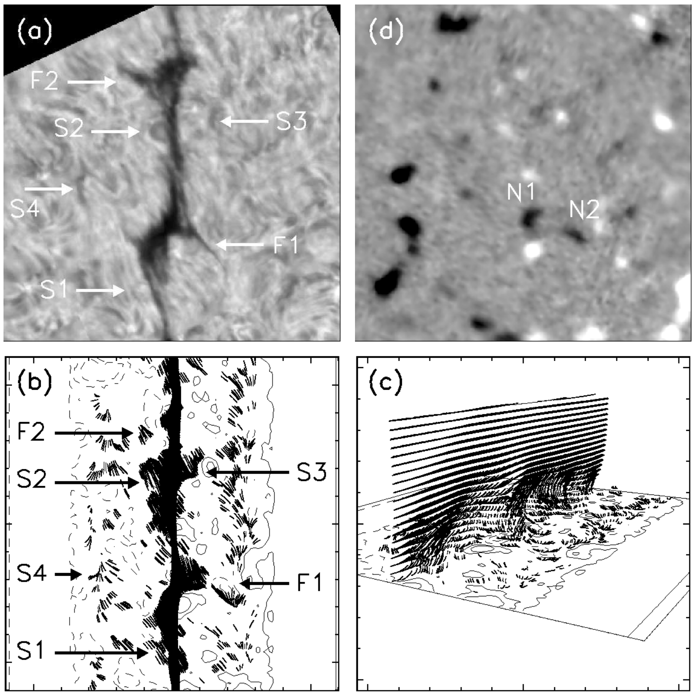

Fig. 8. (**a**) Example of a filament observed in the Hα line-center. Arrows point to particular structures (filament foot or chromospheric fibrils) (**b**) Model of the magnetic configuration computed from the photospheric magnetogram (represented by isocontours). The dark lines correspond to the lower bottom of the 3-D distribution of dipped field lines. (**c**) Side-view of the prominence model. The dark lines correspond only to the bottom of the dips which are supposed to be filled by dense plasma. Even in such a model, the twisted configuration is not apparent (see text). (**d**) Photospheric magnetogram from MDI/SOHO. (From Aulanier et al. 1998)

while arch-filament systems and surges are dynamic plasma structures where dense plasma is forced to move along field lines. In both cases the plasma traces the magnetic flux tubes. At the opposite, during the quiescent phase of prominences the cold plasma fills only the extreme lower part of dipped field lines (a view still under debate !); it is then difficult to relate directly the morphology of the cold plasma to the presence of the magnetic field. It is only when a detailed analysis of the various observations is realized in parallel with a theoretical approach that a coherent picture emerges.

This short description of filaments shows that they are very peculiar structures in the solar atmosphere both from the plasma and magnetic point of view. Still nowadays, the origin and the thermal stability of the cold plasma is a matter of research. Their magnetic structure is also still a matter of debate, partly because measurements of magnetic fields inside prominences yield counter-intuitive results (see below). There is in fact growing evidence that filaments are associated with the strongest non-potentiality of the coronal magnetic field. With the large set of observational techniques available in filaments, they are instructive "probes" of the more complex coronal structures.

5.2 Results from Magnetic-Field Measurements

Prominences are always found above lines where the vertical component of the photospheric magnetic field reverses sign. They are embedded within regions, called corridors or filament channels, which are nearly free of vertical magnetic field flux except small parasitic polarities (e.g. Martin 1990). They are also characterized on either side by the presence of chromospheric fibrils nearly aligned with the inversion line, indicating a high magnetic shear (e.g. Rompolt 1990).

In prominences the Zeeman effect only allows the measurement of the longitudinal component of the magnetic field (see Kim 1990 and references therein). Radio wavelengths provide information on the field strength (e.g. Apushkinskii et al. 1990). The Hanle effect gives the three components of the field (and the electron density) from the polarization measurements in two spectral lines (e.g. Bommier et al. 1994). The compatibility of the results obtained by these three independent methods and by different groups of observers have strongly contributed to validate the results (see Leroy 1988, 1989; Kim 1990).

One of the main results of Hanle measurements is that the prominence field has the opposite direction to the one expected from extrapolation of photospheric measurements (e.g. Leroy et al. 1983). Not only is the field component orthogonal to the prominence opposite to the field of a simple arcade (referred to inverse configuration), but also the field component parallel to the prominence is opposite to those of an arcade that would have been sheared by differential rotation ! This has been shown after a detailed analysis because twin solutions, symmetrical with regard to the line of sight, exist with optically thin lines and right angle scattering (known as 180^0 ambiguity). A large majority of prominences belong to the inverse type (75% in Leroy et al. 1984, 85% in Bommier et al. 1994 and greater than 90% in Bommier and Leroy 1998).

It is now well accepted that the magnetic field in prominences is nearly horizontal, while compatible with a slight magnetic dip (Bommier et al. 1994). The magnetic field strength is nearly homogeneous (Leroy 1989) on the scale of a few arc seconds, but shows a statistical increase of strength with height which is compatible with a large-scale dip configuration (e.g. Leroy et al. 1983).

5.3 Models for Prominence Support

The kind of magnetic configuration supporting filaments is still a matter of debate because the observations of the magnetic field are only partial (at the photosphere and in the prominence). Because filaments are long lived structures (weeks to months) there is clearly the need for a stable support. The most plausible one is the presence of a magnetic dip where dense plasma can be caught to form a filament (Kippenhahn and Schlüter 1957). There are three basic configurations which satisfy this constraint.

In arcade-like magnetic configurations a dip cannot be present in a force-free 2.5-D arcade, since the field lines become only flatter as the magnetic shear increases (Amari et al. 1991). This is however possible in 3-D with an overlying arcade compressing locally the central-part of an underlying sheared arcade (Antiochos et al. 1994). The latter gives mostly an inverse-polarity prominence with a magnetic field nearly aligned with the photospheric inversion line.

The second possibility is a support in quadrupolar configurations. Kippenhahn and Schlüter (1957, in their section 4) first proposed these inverse configurations for stable support of dense plasma. The model was further developed by Malherbe and Priest (1983), Démoulin and Priest (1993), Drake et al. (1993), and Uchida (1998). The presence of a corridor free of significant field is needed to have a prominence extension reaching the chromosphere and converging motions are required to provide mass supply. The quadrupolar model has been extended to magnetic configurations typically found in active regions (Titov et al. 1993; Bungey et al. 1996) and in polar crown regions (Cartledge et al. 1996).

The third possibility, and the most plausible in view of the various observational constraints is the presence of a twisted magnetic configuration. It can be formed in several ways: by photospheric twisting motions (e.g. Priest et al. 1989), by converging motions in a sheared arcade with magnetic reconnection at the inversion line (e.g. van Ballegooijen and Martens 1989), by resistive instability in a sheared arcade (e.g. Inhester et al. 1992), by relaxation and accumulation of magnetic helicity (e.g. Rust and Kumar 1994) or by emergence from the convective zone (e.g. Low 1996). Low and Hundhausen (1995) show how a twisted-flux tube topology can bring together many of the chromospheric and magnetic observations. This was further developed for 3-D configurations by Aulanier and Démoulin (1998a). In particular they could reproduce naturally the feet of prominences which have been a long-standing puzzle (Fig. 8). This model has been successfully tested on an observed filament by computing the magnetic configuration associated to the photospheric magnetograms (Aulanier et al. 1998b).

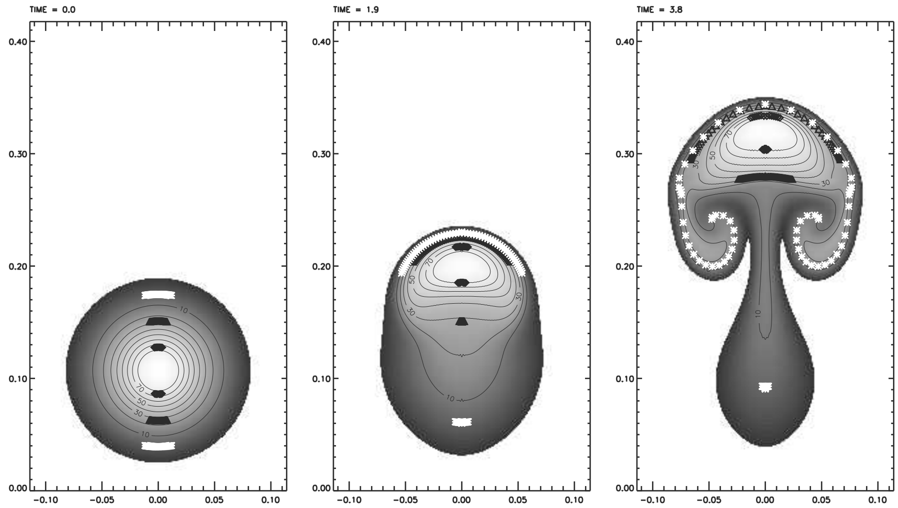

Fig. 9. Rise of a twisted flux tube in the convective zone with an initial magnetic field inclined to the flux tube axis by 7^0. The initial circular flux tube is deformed by the wake. Continuous lines represent isocontours of the field component along the flux tube axis. White and black tracers show the motions of individual plasma elements. (From Emonet and Moreno-Insertis 1998)

6 Global Evolution of Twisted Magnetic-Flux Tubes

6.1 Evolution in the Convective Zone

The amplification of magnetic field by plasma motions (dynamo mechanism) is taking place mainly at the bottom of the convective zone in the convective overshoot region (with a height estimated to $\approx$ 10 Mm). There the subadiabatically stratified plasma provides both plasma motions (in particular differential rotation) and mechanical stability for an intensification of the magnetic field (e.g. Spiegel and Weiss 1980). A Rayleigh-Taylor instability permits to form flux tubes. Above a strength $\approx$ 10 T the flux tube becomes undulatory unstable: the plasma in upward displaced parts moves to the downward displaced parts, leading to a buoyancy force acting upward on the upper parts of the flux tube (e.g. Spruit and van Ballegooijen 1982). Emonet and Moreno-Insertis (1998 and references therein) have shown that a minimum critical twist is needed so that the buoyant flux tube is not destroyed in its rise by the hydrodynamic vortex which develops behind. Moreover, for twist higher than the critical one, the combination of a higher buoyancy force in the central part of the flux tube with the effect of the following roles (in the wake) deform the initial twisted flux tube: it forms a magnetic configuration which has dips not only below the central O point but also on both sides (Fig. 9). These results have been confirmed by Fan et al. (1998).

6.2 Emergence at the Photosphere

So far the MHD simulations studied the deep convection zone and not the emergence through the photosphere of the flux tube. There the hypothesis breaks down: in particular the flux-tube radius becomes larger than the gravitational scale height. One possibility is that the flux tube splits in several smaller flux tubes. It is also not yet fully clear how the mass unloading of the flux tube is realized through this emergence but it is thought to be a difficult and long process (see e.g. Low 1996). The emergence of twisted configurations is supported by recent vector field measurements (Lites et al. 1995; Leka et al. 1996).

6.3 Evolution in the Corona

In the soft X-ray range the Yohkoh satellite provides many examples of S-shaped coronal loops which can be interpreted as the eruption of a twisted structure (see, e.g., Manoharan et al. 1996; Pevtsov et al. 1996; Rust and Kumar 1996). This eruption can be triggered by a loss of equilibrium or a rapid injection of new flux. In the last case, the eruption is driven directly from the emergence without need of pre-stored energy in the corona (Chen 1996), while in the first case, a slow photospheric evolution permits accumulation of energy in the corona long before the loss of equilibrium occurs. A catastrophe may happen in the configuration when a cusp in the equilibrium curve (e.g., twist versus height) is present (e.g. Lin et al. 1998). Finally the eruption of a 3-D twisted magnetic configuration on the sun may have close analogy with flux rope formation occurring in the Earth's magnetotail (e.g. Birn and Hesse 1990)

Many observations suggest a helical-like pattern during eruption of prominences: on the disk (e.g. Raadu et al. 1988) and more often at the limb (e.g. Rompolt 1990; Vršnak et al. 1991). During the quiescent phase, prominences and filaments show little direct evidence of the general magnetic configuration supporting them (see Sec. 5.1). However a model based on the photospheric magnetogram can permit to recover the shape of the prominence with a twisted flux tube (Aulanier et al. 1998b). Moreover the magnetic topology found is basically the one found independently in MHD simulations of Emonet and Moreno-Insertis (1998, see in Sec. 6.1) !

6.4 Ejection in the Interplanetary Space

Observation of CMEs can be frequently associated to the eruption of a prominence. This relationship is confirmed both by the detailed examination of well-observed events and by statistical analysis (e.g. Hundhausen 1988). In coronograph pictures the prominence embedded within the coronal CME material often displays a distinctly twisted structure which strongly suggests a flux rope structure of the expanding magnetic field. Other but morphological evidence for this comes e.g. from radio observations. In a limb event Klein and Mouradian (1991) observed that the structure initially seen as a rising prominence shows later up as a radio source where confined electrons rise, pursuing the trajectory of the rising prominence in a uniformly accelerated ascending motion that extends over several solar radii. The prolonged confinement of the electrons suggests the presence of flux rope type twisted field lines in the rising structure. In some particularly favorable observations the ejection can be followed to large distances: with different instruments, Jackson et al. (1988) have followed a prominence eruption and the associated CME from the solar surface up to 100 $R_\odot$!

The twisted magnetic flux tube is also in agreement with the topology inferred for CMEs from coronagraph observation(e.g. Hundhausen 1988; Chen et al. 1997; Simnett et al. 1997). In the interplanetary medium, twisted configurations are also identified in magnetic clouds (or interplanetary CMEs) with in situ measurements from Ulysses (e.g. Bothmer et al. 1996; Weiss et al. 1996; Farrugia 1997; Osherovich and Burlaga 1997). The link between magnetic clouds, CMEs and prominence eruptions is highly probable both on a statistical ground (e.g. Bothmer and Schwenn 1994; Marubashi 1997) and from the detailed study of individual cases (e.g. Burlaga et al. 1998).

In conclusion, observational evidence and theoretical investigations from the convective zone to the interplanetary space are in favor of the formation and subsequent ejection of twisted flux tubes (After all they are natural configurations for a stressed magnetic field !). The twisted flux tubes, probably formed at the bottom of the convective zone, bring both magnetic energy and helicity in the corona. In a highly conductive medium like the corona, magnetic energy can be dissipated at a fast rate (which is only weakly dependent on the magnetic Reynolds number), while magnetic helicity is a well preserved quantity (see Biskamp 1993). In this way energy release, which is confined in the corona, permits to get rid of part of the magnetic energy excess but cannot remove the magnetic helicity (and the associated excess of magnetic energy). Most of this helicity cannot be removed by cancellation of opposite helicities because the sign of helicity is mainly hemisphere dependent (negative/positive in the north/south hemisphere) without the reversal of sign observed for the magnetic field itself after each solar cycle (11 years). The only way the sun has to get rid of the accumulated magnetic helicity is then by ejecting it in the interplanetary medium (Low 1996). Such evolution (from the formation to the ejection) of twisted flux tubes is a natural, though complex, consequence of the MHD equations.

References

1. Alissandrakis, C.E. (1994). In: Belvedere, G., Rodonó, M., Simnett, G.M. (Eds.) Advances in Solar Physics, Lecture Notes in Physics, Springer, Berlin, **432**, 109
2. Alissandrakis, C.E., Tsiropoula, G., Mein, P. (1990) A&A **230**, 200

3. Aly, J.J. (1987). In: Beck, R., Gräve, R. (Eds.) Interstellar Magnetic Fields, Springer Verlag, Berlin, 240
4. Aly, J.J. (1990). In: Dezsõ, L. (Ed.) The Dynamic Sun, Public. Debrecen Obs., 176
5. Aly, J.J. (1991) ApJ **375**, L61
6. Aly, J.J. (1995) ApJ **439**, L63
7. Amari, T., Démoulin, P., Browning, P., et al. (1991) A&A **241**, 604
8. Amari, T., Luciani, J.F., Aly, J.J., Tagger, M. (1996) ApJ **446**, L39
9. Amari, T., Luciani, J.F., Aly, J.J., Mikić, Z. (1997a). In: Crooker, N. Joselyn, J.A., Feynman, J. (Eds.) Coronal mass ejections, American Geophysical Union, 101
10. Amari, T., Aly, J.J., Luciani, J.F., Boulmezaoud, T., Mikić, Z. (1997b) Solar Phys. **174**, 129
11. Antiochos, S.K. (1987) ApJ **312**, 886
12. Antiochos, S.K., Dahlburg, R.B., Klimchuck, J.A. (1994) ApJ **420**, L41
13. Apushkinskii, G.P., Nesterov, N.S., Topchilo, N.A., Tsyganov, A.N. (1990), SvA, **34(5)**, 530
14. Aulanier, G., Démoulin, P. (1998a) A&A **329**, 1125
15. Aulanier, G., Démoulin, P., van Driel-Gesztelyi, L., et al. (1998b) A&A **335**, 309
16. Aulanier, G., Démoulin, P., Schmieder, B., et al. (1998c) Solar Phys. in press
17. Berger, M.A. (1991) A&A **252**, 369
18. Benz, A.O. (1993) Plasma Astrophysics, Kluwer
19. Bird, M.K., Edenhofer, P. (1990). In: Harve Schwenn, R., Marsch, E. (Eds.) Physics of the Inner Heliosphere Vol. 1, Springer, Berlin, Heidelberg, New York, 13
20. Birn, J., Hesse, M. (1990) Geophys. Monogr. Ser., **58**, 655
21. Birn, J., Hesse, M., Schindler, K. (1996) JGR **101, A6**, 12939
22. Biskamp, D. (1993) Non linear MHD, Cambridge University Press, Cambridge
23. Bommier, V., Leroy, J.L. (1998). In: Webb, D., Schmieder, B., Rust, D. (Eds.) IAU Colloq. 167, Astronomical Society of the Pacific, **150**, 434
24. Bommier, V., Landi Degl'Innocenti, E., Leroy, J.L., Sahal-Bréchot S. (1994) Solar Phys. **154**, 231
25. Bothmer, V., Schwenn, R. (1994) Spa. Sci. Rev., **70**, 215
26. Bothmer, V., Desai, M.I., Marsden, R.G., et al. (1996) A&A **316**, 493
27. Bungey, T.N., Titov, V.S., Priest, E.R., (1996) A&A **308**, 233
28. Burlaga, L., Fitzenreiter, Lepping, R., et al. (1998) JGR **103, A1**, 277
29. Cartledge, N.P., Titov, V.S., Priest, E.R. (1996) Solar Phys. **166**, 287
30. Chen, J. (1996) JGR **101**, 27499
31. Chen, J., Howard, R.A., Brueckner, G.E., et al. (1997) ApJ **490**, L191
32. Chou, D.Y., D.Y., Zirin, H. (1988) ApJ **333**, 420
33. Cox, A.N., Livingston, W.C., Matthews, M.S. (Eds.), (1991) Solar Interior and Atmosphere, The Univ. Arizona Press, Tucson
34. Crooker, N., Joselyn, J.A., Feynman, J. (Eds.), (1997) Coronal mass ejections, Geophysical Monograph Series
35. David, C., Gabriel, A.H., Bely-Dubau, F., et al. (1998) A&A **336**, L90
36. Démoulin, P., Priest, E.R. (1993) Solar Phys. **144**, 283
37. Démoulin, P., Priest, E.R. (1997) Solar Phys. **175**, 123
38. Démoulin, P., Hénoux, J.C., Mandrini, C.H. (1994) A&A **285**, 1023

39. Démoulin, P., Hénoux, J.C., Priest, E.R., Mandrini, C.H. (1996a) A&A **308**, 643
40. Démoulin, P., Priest, E.R., Lonie, D.P. (1996b) JGR **101**, A4, 7631
41. Démoulin, P., Bagalá, L.G., Mandrini, C.H., et al. (1997) A&A **325**, 305
42. Dmitruk, P., Gómez, D.O. (1997) ApJ **484**, L83
43. Drake, J.F., Mok, Y., van Hoven, G. (1993) ApJ **413**, 416
44. Dreher, J., Birk, G.T., Neukirch, T. (1997) A&A **323**, 593
45. Einaudi, G. (1998) this volume
46. Einaudi, G., Velli M. (1994). In: Belvedere, G., Rodonó, M., Simnett, G.M. (Eds.) Advances in Solar Physics, Lecture Notes in Physics, Springer, Berlin, **432**, 149
47. Emonet, T., Moreno-Insertis, F. (1998) ApJ **492**, 804
48. Fan, Y., Zweibel, E.G., Lantz, S.R. (1998) ApJ **493**, 480
49. Farrugia, C.J. (1997). In: Crooker, N. Joselyn, J.A., Feynman, J. (Eds.) Coronal mass ejections, American Geophysical Union, 177
50. Finn, J.M., Lau, Y.T. (1991) Phys. Fluids **B3**, 2675
51. Fontaine, D. (1998) this volume
52. Forbes, T.G., Acton, L.W. (1996) ApJ **459**, 330
53. Georgoulis, M.K., Velli, M., Einaudi, G. (1998) ApJ **497**, 957
54. Golub, L., Pasachoff, Jay M. (1997) The Solar Corona, Cambridge University Press
55. Golub, L., Harvey, J.W., Webb, D.F. (1986). In: Poland, A.I. (Ed.), Coronal and Prominence Plasmas, NASA CP-2442, 365
56. Golub, L., Krieger, A.S., Harvey, J.W., Vaiana, G.S. (1977) Solar Phys. **53**, 111
57. Goossens, M. (1991). In: Priest, E.R., Hood, A. W. (Eds.) , Advances in Solar System Magnetohydrodynamics, Cambridge University Press, Cambridge 137
58. Gómez, D.O. (1990) Fund. Cosmic Phys., **14**, 131
59. Gómez, D.O., DeLuca, E.E., Mc Clymont, A.N. (1995) ApJ **448**, 954
60. Hanaoka, Y. (1995) Solar Phys. **165**, 275
61. Harvey, K.L., Nitta, N., Strong, K.T., Tsuneta, S. (1994). In: Uchida, Y., Watanabe, T. Shibata, K., Hudson, H.S. (Eds.) X-ray Solar Physics from Yohkoh, Frontiers Science Series, **10**, 21
62. Heikkila, W.J. (1997) JGR **102, A5**, 9651
63. Heyvaerts, J. (1998) this volume
64. Heyvaerts, J., Priest, E.R. (1983) A&A **117**, 220
65. Heyvaerts, J., Priest, E.R. (1984) A&A **137**, 63
66. Heyvaerts J., Priest E.R., Rust D.M. (1977) ApJ **216**, 123
67. Hesse, M., Birn, J., Hoffman, R.A. (1997) JGR **102, A5**, 9543
68. Hollweg, J.V. (1990) Comput. Phys. Rep., **12**, 205
69. Hundhausen, A.J. (1988). In: Pizzo, V.J., Holzer, T.E., Sime, D.G. (Eds.) Solar Wind 6, NCAR TN-306, Boulder **1**, 181
70. Inhester, B., Birn, J., Hesse, M. (1992) Solar Phys. **138**, 257
71. Inverarity, G.W., Priest, E.R. (1995) A&A **302**, 596
72. Jackson, B., Rompolt, B., Svestka, Z. (1988) Solar Phys. **115**, 327
73. Kim, I.S. (1990). In: Ruždjak, V., Tandberg-Hanssen, E. (Eds.) IAU Colloq. 117, Springer, Berlin, 49
74. Kippenhahn, R., Schlüter, A. (1957) Zs. Ap. **43**, 36

75. Klein, K.-L. (1992). In: Méthodes de détermination des champs magnétiques solaires et stellaires, Faurobert–Scholl, M., Frisch, H., Mein, N. (Eds.) Publ. Obs. Paris, 113
76. Klein, K.-L., Mouradian, Z. (1991). In: Schmieder, B., Priest, E.R. (Eds.) Proc. Chantilly Meeting on Solar Flares, Publ. Obs. Paris, 185
77. Koutchmy, S. (1994) Adv. Space Res. **14(4)**, 29
78. Kundu, M.R., Strong, K.T., Pick, M., et al. (1994) ApJ **427**, L59
79. Lau, Y.T. (1993) Solar Phys. **148**, 301
80. Leka, K.D., Canfield, R.C., McClymont, A.N., van Driel-Gesztelyi, L. (1996) ApJ **462**, 547
81. Leroy, J.L. (1988). In: Altrock, R.C. (Ed.) Solar and Stellar coronal structures and dynamics, National Solar Observatory, 422
82. Leroy, J.L. (1989). In: Priest, E.R. (Ed.) Dynamics and Structure of Quiescent Solar Prominences, Kluwer, Dordrecht, 77
83. Leroy, J.L., Bommier, V., Sahal-Bréchot, S. (1983) Solar Phys. **83**, 135
84. Leroy, J.L., Bommier, V., Sahal-Bréchot, S. (1984) A&A **131**, 33
85. Lin, J., Forbes, T.G., Isenberg, P.A., Démoulin, P. (1998) ApJ **417**, 368
86. Linker, J.A., Mikić, Z. (1995) ApJ **438**, L45
87. Lites, B.W., Low, B.C., Martinez Pillet, V., et al. (1995) ApJ **446**, 877
88. Longcope, D.W., Strauss, H.R. (1994) ApJ **437**, 851
89. Longcope, D.W., Sudan, R.N. (1992) ApJ **384**, 305
90. Low, B.C. (1992) A&A **253**, 311
91. Low, B.C. (1996) Solar Phys. **167**, 217
92. Low, B.C., Hundhausen, J.R. (1995) ApJ **443**, 818
93. Low, B.C., Wolfson, R. (1988) ApJ **324**, 574
94. Lynden-Bell, D., Boily, C. (1994) Mon. Not. R. Astron. Soc., **267**, 146
95. Machado, M.E., Moore, R.L., Hernández, A.M., et al. (1988) ApJ **326**, 425
96. Malherbe, J.M., Priest, E.R. (1983) A&A **123**, 80
97. Malherbe, J.M., Tarbell, T., Wiik, J.E., et al. (1997) ApJ **482**, 535
98. Mandrini, C.H., Démoulin, P., van Driel-Gesztelyi, L., et al. (1996) Solar Phys. **168**, 115
99. Mandrini, C.H., Démoulin, P., Bagalá, L.G., et al. (1997) Solar Phys. **174**, 229
100. Manoharan, P.K., van Driel-Gesztelyi, L., Pick, M., Démoulin, P. (1996) ApJ **468**, L73
101. Martin, S.F. (1990). In: Ruždjak, V., Tandberg-Hanssen, E. (Eds.) IAU Colloq. 117, Springer-Verlag, Berlin, 1
102. Martin, S.F., Livi, S.H.B., Wang, J., Shi, Z. (1985). In: Hagyard, M.J. (Ed.) Measurements of Solar Vector Magnetic Fields, NASA CP-2374, 403
103. Martens, P.C.H., Van den Oord, G.H.J., Hoyng P. (1985) Solar Phys. **96**, 253
104. Marubashi, K. (1997). In: Crooker, N. Joselyn, J.A., Feynman, J. (Eds.) Coronal mass ejections, American Geophysical Union, 147
105. Mc Clymont, A.N., Jiao, L., Mikić, Z. (1997) Solar Phys. **174**, 191
106. Mein, P., Démoulin, P., Mein, N., et al. (1996) A&A **305**, 343
107. Melrose D.B., Khan J.I. (1989) A&A **219**, 308
108. Mercier, C., Heyvaerts, J. (1977) A&A **61**, 685
109. Metcalf, T.R., Canfield, R.C., Hudson, H.S., et al. (1994) ApJ **428**, 860
110. Mikić, Z., Schnack, D.D., Van Hoven, G. (1989) ApJ **338**, 1148
111. Mikić, Z., Linker, J.A. (1994) ApJ **430**, 898
112. Moore, R.L., La Rosa, T.N., Orwig, L.E. (1995) ApJ **438**, 985

113. Nolte, J.T., Solodyna, C.V., Gerassimenko, M. (1979) Solar Phys. **63**, 113
114. Osherovich, V., Burlaga, L.F. (1997). In: Crooker, N. Joselyn, J.A., Feynman, J. (Eds.) Coronal mass ejections, American Geophysical Union, 157
115. Parker, E.N. (1972) ApJ **174**, 499
116. Parker, E.N. (1990) Geophys. Astrophys. Fluid Dyn. **52**, 183
117. Parker, E.N. (1994) Spontaneous Current Sheets in Magnetic Fields, Oxford University Press, Oxford
118. Parker, E.N. (1996) JGR **101, A5**, 10587
119. Parker, E.N. (1997) JGR **102, A5**, 9657
120. Parnell, C.E. (1998) this volume
121. Parnell, C.E., Priest, E.R., Golub, L. (1994) Solar Phys. **151**, 57
122. Pevtsov, A.A., Canfield, R.C., Zirin, H. (1996) ApJ **473**, 533
123. Priest, E.R. (1982) Solar Magneto-hydrodynamics, D. Reidel, Dordrecht
124. Priest, E.R., Démoulin, P. (1995) JGR **100**, A12, 23443
125. Priest, E.R., Forbes, T.G. (1990) Solar Phys. **126**, 319
126. Priest, E.R., Forbes, T.G. (1992) JGR **97**, A11, 16757
127. Priest, E.R., Hood, A.W., Anzer, U. (1989) ApJ **344**, 1010
128. Raadu, M.A., Schmieder, B., Mein, N., Gesztelyi, L. (1988) A&A **197**, 289
129. Rompolt, B. (1990), Hvar Obs. Bull. Vol. **14, 1**, 37
130. Rust, D.M., Kumar, A. (1994) Solar Phys. **155**, 69
131. Rust, D.M., Kumar, A. (1996) ApJ **464**, L199
132. Sams, III B.J., Golub, L., Weiss, N.O. (1992) ApJ **399**, 313
133. Schindler, K., Hesse, M., Birn, J. (1988) JGR **93**, 5547
134. Schmelz, J.T., Brown, J.C. (1992) The Sun - A Laboratory for Astrophysics, NATO ASI Series, Kluwer
135. Schmieder, B. (1992). In: Svestka, Z., Jackson, B.V., Machado, M.E., (Eds.) Eruptive solar flares, Lecture Notes in Physics, Springer, Berlin. 124
136. Schmieder, B., Démoulin P., Aulanier G., Golub L. (1996) ApJ **467**, 881
137. Schmieder, B., Aulanier, G., Démoulin, P., et al. (1997) A&A **325**, 1213
138. Schwenn, R. (1990). In: Schwenn, R., Marsch, E. (Eds.) Physics of the Inner Heliosphere Vol. 1, Springer, Berlin, Heidelberg, New York, 99
139. Shimizu, T., Tsuneta, S., Acton, L.W., et al. (1994) ApJ **422**, 906
140. Simnett, G.M., Tappin, S.J., Plunkett, S.P., et al. (1997) Solar Phys. **175**, 685
141. Somov, B.V. (1992) Solar Flares, Springer, Berlin
142. Spiegel, E.A., Weiss, N.O. (1980) Nat **287**, 616
143. Spruit, H.C., van Ballegooijen A.A. (1982) A&A **106**, 58
144. Stenflo, J.O. (1994) Solar Magnetic Fields – Polarized Radiation Diagnostics, Kluwer, Dordrecht
145. Stix, M. (1991) The Sun, An Introduction, Springer, Berlin
146. Strong, K.T., Harvey, K.L., Hirayama, T., et al. (1992) Publ. Astron. Soc. Japan, **44**, L161
147. Sturrock, P.A. (1991) ApJ **380**, 655
148. Sturrock, P.A., Antiochos S.K., Roumeliotis G. (1995) ApJ **443**, 804
149. Tandberg-Hanssen, E., Emslie, A.G. (1988) The Physics of Solar Flares, Cambridge University Press, Cambridge, UK
150. Tandberg-Hanssen, E. (1995) The Nature of Solar Prominences, Kluwer, Dordrecht
151. Titov, S., Priest, E.R., Démoulin, P. (1993) A&A **276**, 564

152. Tu, C.-Y., Marsch, E., Wilhelm, K., Curdt, W. (1988) ApJ **503**, 475
153. Uchida, Y. (1998). In: Webb, D., Schmieder, B., Rust, D. (Eds.) IAU Colloq. 167, Astronomical Society of the Pacific, **150**, 163
154. van Ballegooijen, A.A. (1986) ApJ **311**, 1001
155. van Ballegooijen, A.A. (1988) Geophys. Astrophys. Fluid Dyn. **41**, 181
156. van Ballegooijen, A.A., Martens, P.C.H. (1989) ApJ **343**, 971
157. van Driel-Gesztelyi, L., Schmieder, B., Cauzzi, G., et al. (1996) Solar Phys. **163**, 145
158. van Driel-Gesztelyi, L., Wiik, J.E., Schmieder, B., et al. (1997) Solar Phys. **174**, 151
159. van Speybrock, L.P., Krieger, A.S., Vaiana, G.S. (1970) Nat **227**, 818
160. Vekstein, G.E. Priest, E.R. (1992) ApJ **384**, 333
161. Vekstein, G.E., Priest, E.R., Amari, T. (1991) A&A **243**, 492
162. Vršnak, B., Ruždjak, V., Rompolt, B. (1991) Solar Phys. **136**, 151
163. Webb, D.F., Martin, S.F., Moses, D., Harvey, J.W. (1993) Solar Phys. **144**, 15
164. Weiss, L.A., Gosling, J.T., Mc Allister, A.H., et al. (1996) A&A **316**, 384
165. Wilhelm, K., Marsch, E., Dwivedi, B.N., et al. (1998) ApJ **500**, 1023
166. Withbroe, G.L. (1988) ApJ **325**, 442
167. Wolfson, R. (1989) ApJ **344**, 471
168. Wolfson, R., Bhattacharjee, H., Dlamini, B. (1996) ApJ **463**, 359
169. Woo, R.T., Armstrong, J.W., Bird, M.K., Pätzold, M. (1995) ApJ **449**, L91
170. Yoshida, T., Tsuneta, T. (1996) ApJ **459**, 342
171. Zweibel, E.G., Li, H.S. (1987) ApJ **312**, 423
172. Zwingmann, W., Schindler, K., Birn, J. (1985) Solar Phys. **99**, 133